Article

Multi-Walled Carbon Nanotube-Doped Tungsten Oxide Thin Films for Hydrogen Gas Sensing

Chatchawal Wongchoosuk [1], Anurat Wisitsoraat [2], Ditsayut Phokharatkul [2], Adisorn Tuantranont [2] and Teerakiat Kerdcharoen [1,3,*]

[1] Department of Physics and Center of Nanoscience and Nanotechnology, Faculty of Science, Mahidol University, Ratchathewee, Bangkok 10400, Thailand; E-Mail: g5037004@student.mahidol.ac.th

[2] Nanoelectronics and MEMS Laboratory, National Electronics and Computer Technology Center, Klong Luang, Pathumthani 12120, Thailand; E-Mails: anurat.wisitsoraat@nectec.or.th (A.W.); ditsayut.phokharatkul@nectec.or.th (D.P.); adisorn.tuantranont@nectec.or.th (A.T.)

[3] NANOTEC Center of Excellence at Mahidol University, National Nanotechnology Center, Thailand

* Author to whom correspondence should be addressed; E-Mail: sctkc@mahidol.ac.th; Tel.: +6-622-015-770; Fax: +6-622-015-843.

Abstract: In this work we have fabricated hydrogen gas sensors based on undoped and 1 wt% multi-walled carbon nanotube (MWCNT)-doped tungsten oxide (WO_3) thin films by means of the powder mixing and electron beam (E-beam) evaporation technique. Hydrogen sensing properties of the thin films have been investigated at different operating temperatures and gas concentrations ranging from 100 ppm to 50,000 ppm. The results indicate that the MWCNT-doped WO_3 thin film exhibits high sensitivity and selectivity to hydrogen. Thus, MWCNT doping based on E-beam co-evaporation was shown to be an effective means of preparing hydrogen gas sensors with enhanced sensing and reduced operating temperatures. Creation of nanochannels and formation of p-n heterojunctions were proposed as the sensing mechanism underlying the enhanced hydrogen sensitivity of this hybridized gas sensor. To our best knowledge, this is the first report on a MWCNT-doped WO_3 hydrogen sensor prepared by the E-beam method.

1. Introduction

Hydrogen (H_2) is one of the most useful gases, being used in many chemical processes and various industries including aerospace, medical, petrochemical, transportation, and energy [1-3]. In recent years, H_2 has attracted a great deal of attention as a potential clean energy source for the next generation of automobiles and household appliances due to its perfectly clean combustion without any release of pollutants or greenhouse gases [4]. However, this low molecular weighted gas can easily leak out and may cause fires or explosions when its concentration in air is between 4% and 75% by volume [5]. Moreover, H_2 is a colorless, odorless and tasteless gas that cannot be detected by human senses. Therefore, it is very essential to develop the effective H_2 gas sensors for monitoring of H_2 leaks.

Tungsten Oxide (WO_3) is one of the most widely studied gas-sensing materials due to its fast, high sensitivity response toward NO_x [6-9], H_2S [10-13], C_2H_5OH [13,14] CO [15], NH_3 [15-19] and O_3 [20]. In case of H_2 detection, it is well known that H_2 molecules are not activated on the smooth WO_3 surface of single crystals [21]. Addition of some noble metals such as Pt, Pd, or Au [22-26] to WO_3 usually improves the sensitivity and selectivity to H_2 gas. These metal doped WO_3 films can be prepared by several methods, including screen printing [22], sputtering [23,24] and sol-gel process [25,26].

In the present work, multi-walled carbon nanotube (MWCNT)-doped WO_3 thin films fabricated by an electron beam (E-beam) evaporation process and their application for H_2 gas sensing are reported for the first time. The E-beam process offers extensive possibilities for controlling film structure and morphology with desired properties such as dense coating, high thermal efficiency, low contamination, high reliability and high productivity. MWCNTs were selected for doping because of their larger effective surface area, with many sites available to adsorb gas molecules, and their hollow geometry that may be helpful to enhance the sensitivity and reduce the operating temperature. Furthermore, MWCNTs were reported to be sensitive to H_2, with good recovery times [27].

2. Experimental

2.1. Preparation of Materials

Commercial WO_3 powder was obtained from Merck and used without further purification. MWCNTs were grown by the thermal chemical vapor deposition (CVD) process. The catalyst layer of aluminium oxide (10 nm) and stainless steel (5 nm) was deposited on the silicon (100) substrates (Semiconductor Wafer Inc.) using reactive sputtering apparatus. The synthesis of MWCNTs was performed under a flow of acetylene/hydrogen at a ratio of 3.6:1 at 700 °C for 3 min. To obtain high-purity MWCNTs, the water-assisted selective etching technique [28] was applied after each CNT's growth stage. Water vapor (300 ppm) was introduced into the system by bubbling argon gas through liquid water at room temperature for 3 min. The sequence of acetylene/hydrogen and water vapor flows was repeated for five cycles. Based on the scanning electron microscopic (SEM) image, as shown in Figure 1, the diameter and length of the MWCNTs are ~35 nm and ~26 μm, respectively. The electrical conductivity of MWCNTs was ~75 S/cm, as measured by a four-point probe method at room temperature. In addition, high-resolution transmission electron microscopic (HR-TEM) imaging,

as shown in Figure 2, confirms that CNTs are multi-walled, with the width and number of walls being ~4.6 nm and 14, respectively. Thus, the spacing between two graphitic layers is ~0.33 nm, which is in good agreement with theoretical and experimental values.
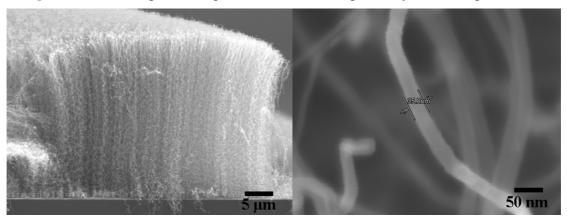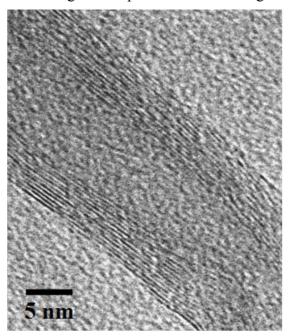
Figure 1. SEM images of the produced MWCNTs grown by the CVD process.

Figure 2. High resolution TEM image of the produced MWCNT grown by the CVD process.

2.2. Fabrication of MWCNTs-doped WO₃ Thin Film

MWCNT-doped WO_3 thin film was fabricated by the E-beam evaporation technique onto Cr/Au interdigitated electrodes on an alumina substrate [29]. The target was prepared by mixing 99 wt% of WO_3 powder with 1 wt% of MWCNT powder using a grinder in a mortar for 30 min and then pelletizing with a hydraulic compressor. Deposition was performed at a pressure of 5×10^{-6} Torr in the evaporation chamber. The substrate was rotated and kept at 130 °C during the deposition in order to obtain a homogeneous thin film. The deposition rate was 2 Å/sec and the final film thickness was 150 nm, as controlled by a quartz crystal monitor. After E-beam evaporation, the film was

annealed at 500 °C for 3 h in air to stabilize the crystalline structure. In addition, an undoped WO$_3$ thin film was also fabricated using the same conditions for comparison.

2.3. Measurement of Gas Sensing

To evaluate the gas sensing properties of the thus prepared thin films, MWCNT-doped WO$_3$ and undoped WO$_3$ gas sensors were placed inside a stainless steel chamber and the resistance measured using a 8846A Fluke multimeter with 6.5 digit resolution. The gas sensing measurements were made within a dynamic flow system with control of sensor operating temperatures (200–400 °C) under variable gas concentrations (100–50,000 ppm). Hydrogen (H$_2$), ethanol (C$_2$H$_5$OH), methane (CH$_4$), acetylene (C$_2$H$_2$), and ethylene (C$_2$H$_4$) were used to test the sensing properties and selectivity of the thin films. The sample gas flow time and the clean air reference flow time were fixed at 5 min and 15 min, respectively. It should be noted that these switching interval was selected so that the resistance change is at least 90% of the saturated value. The sensor resistances were sampled and recorded every second using LabVIEW with a USB DAQ device for subsequent analyses.

3. Results and Discussion

3.1. Characterization of Thin Films

Surface morphology, particle size and crystalline structure of the films were characterized by SEM and TEM. Figure 3 shows the SEM surface morphology of MWCNT-doped WO$_3$ thin film deposited on an alumina substrate. It was seen that the film coated on the rough alumina substrate has approximate grain sizes ranging from 40 to 80 nm.
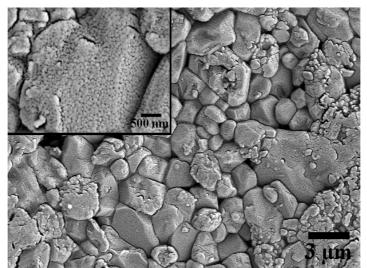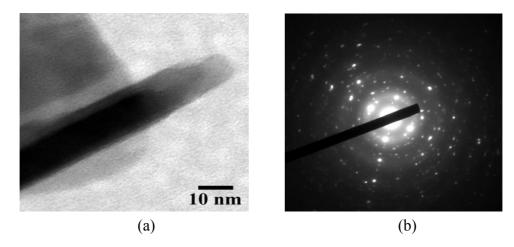
Figure 3. SEM image of MWCNT-doped WO$_3$ thin films on alumina substrate.

The nanometer grain size together with the roughness of the alumina substrate can enhance the gas sensitivity of thin films [30,31] because more gas adsorption sites are available due to the increased surface area and porosity. With the SEM resolution, CNT structure cannot be observed on the thin film surface. Therefore, TEM characterization was used to confirm CNT inclusion into the WO$_3$ film. It should be noted that copper TEM grid samples were loaded inside the evaporation chamber for sample

deposition at the same time as coating on the Cr/Au interdigitated electrodes. TEM observation clearly shows CNT inclusion into the nanocrystalline WO_3, while the electron diffraction pattern exhibits polycrystalline phase in the film, as shown in Figure 4a,b, respectively.

Figure 4. (a) High-resolution TEM image and **(b)** corresponding selected area diffraction pattern of MWCNT-doped WO_3 thin film.

(a)   (b)

The film morphology obtained in our study is in accordance with observations on nanocrystalline WO_3 films grown by other methods [32,33]. Doping of CNT does not change the phase or surface morphology of the film, but it may help form nanochannels in WO_3 films, leading to the enhancement of the sensitivity and reduction of the operating temperature.

3.2. Sensing Properties of Thin Films

The sensor response (S) of the thin films is defined as the percentage of resistance change:

$$S(\%) = \left(\frac{R_0 - R}{R_0} \right) \times 100$$

(1)

where R_0 and R are the resistance of the thin films in pure air and test gas, respectively. Figure 5 shows the response of the undoped WO_3 and MWCNT-doped WO_3 thin films to 1,000 ppm H_2 at varying operating temperatures. It can be seen that the response of the films increases as the operating temperature increases up to 350 °C, and then decreases. The gas-sensing response increases with temperature in the 200–350 °C range because thermal energy helps the reactions involved overcome their respective activation energy barriers [34,35]. However, if the operating temperature becomes too high (*i.e.*, >350 °C), the adsorbed oxygen species at the sensing sites on the film surface will be diminished and less available to react with H_2 molecules [36], thereby limiting the film's response.
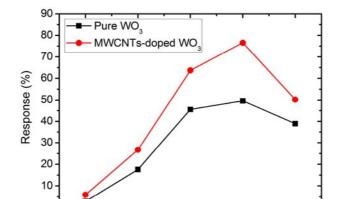
Figure 5. Sensing response to H_2 (1,000 ppm) at different operating temperatures.

At any operating temperature, the sensor response of the MWCNT-doped WO_3 thin film is higher than that of the undoped WO_3 thin film. Specifically, at the optimum operating temperature (350 °C), MWCNT-doped WO_3 thin film yields a 26.9 % higher response than the undoped one. The doped sensor prepared in this work also shows higher response than the WO_3 films prepared by the sol–gel process [25].
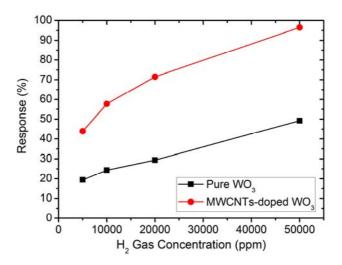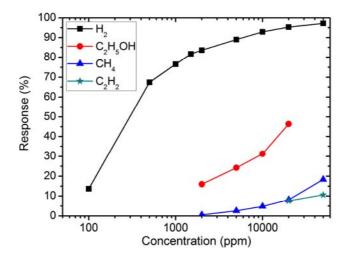
Figure 6. Sensing response of the undoped WO_3 and MWCNT-doped WO_3 thin films to high H_2 concentrations (5,000–50,000 ppm) at the operating temperature of 250 °C.

One major advantage of MWCNT-doped WO_3 thin film is that the sensor can be operated at a lower operating temperature (250 °C), especially if this sensor is used to measure the H_2 gas at higher concentrations (5,000–50,000 ppm). As shown in Figure 6, at such a concentration range, there are sufficient numbers of H_2 molecules available to react with the surface oxygen adsorption sites. It is also well-known that MWCNTs contribute to the reduction of sensor resistance of metal oxides [37] and the activation energy between the WO_3 surface and H_2 gas. The details of the sensing mechanisms of MWCNT-doped WO_3 thin films will be discussed in the next section.

To demonstrate the selectivity of the MWCNT-doped WO$_3$ thin film, its sensing response (at the operating temperature of 350 °C) to various gas vapors, namely H$_2$, C$_2$H$_5$OH, CH$_4$, and C$_2$H$_2$, was measured and plotted (Figure 7). It can be seen that MWCNT-doped WO$_3$ thin film exhibits a strong response to H$_2$, and much weaker responses to C$_2$H$_5$OH, CH$_4$, and C$_2$H$_2$. In particular, this thin film was found to be insensitive to C$_2$H$_4$ at the optimum operating temperature of 350 °C. It is therefore concluded that the MWCNT-doped WO$_3$ thin film exhibits high selectivity to H$_2$.

Figure 7. Sensing response of MWCNT-doped WO$_3$ thin film at the operating temperature of 350 °C to various concentrations of different gas vapors.

3.3. Sensing Mechanism of MWCNTs-doped WO$_3$ Thin Film

It is well known that WO$_3$ is an n-type semiconductor while CNT is a p-type semiconductor. MWCNT-doped WO$_3$ thin film can be either p-type or n-type semiconductors depending on the quantity of MWCNTs and the operating temperature [38]. In this work, the produced MWCNTs-doped WO$_3$ thin film behaves as an n-type semiconductor since the electrical conductivity of the film increases when reducing gases, *i.e.*, H$_2$, are absorbed by its surface. Doping of MWCNTs into the WO$_3$ matrix can introduce nanochannels and form p-n heterojunctions in the thin film. These nanochannels play an important role for gas diffusion. The gas molecules can easily transport into the gas-sensing layers leading to increasing sensitivity [39,40]. In addition, MWCNT-doped WO$_3$ thin film p-n heterojunctions could be formed at the interface between WO$_3$ and the MWCNTs [38,41]. When H$_2$ gas is exposed to MWCNT-doped WO$_3$ thin film, the widths of the depletion layers at the p-n heterojunctions can be modulated. The potential barriers at the interfaces or inside the WO$_3$ may be changed. This change of the depletion layer in the p–n heterojunctions of MWCNT-doped WO$_3$ thin film may explain the enhanced response of the film at low operating temperatures. Various oxygen species chemisorbed at the thin film surface such as O^{2-}, O$_2^-$, and O$^-$ are available for catalytic reactions with H$_2$, thus depending on the temperature at the metal oxide surface [42]. At the operating temperature range of 200–400 °C, O$^-$ is commonly chemisorbed. Consequently, the chemical reaction underlying the H$_2$ gas sensing in this study is given by [43]:

$$H_2 + O_{ads}^- \rightarrow H_2O + e^-$$

(2)

The adsorbed O⁻ on the thin film surface reacts with the H_2 gas yielding H_2O and releasing electrons which contribute to the current increase through the thin film that causes the electrical conductivity to increase.

4. Conclusions

MWCNT-doped WO_3 thin film was successfully prepared by the E-beam evaporation technique. The 1 wt% MWCNT-doped WO_3 thin film exhibits n-type semiconductor behavior of the polycrystalline phase. Doping with MWCNTs does not significantly change any phase or surface morphology of the film, but it introduces nanochannels and form p-n heterojunctions in the WO_3 matrix. The MWCNT-doped WO_3 thin film exhibits high selectivity and sensitivity to H_2 over a relatively wide range of concentrations (100-50,000 ppm). Moreover, it can operate at a relatively low temperature. This should be useful for developing high performance H_2 gas sensors. To our best knowledge, this is the first report on MWCNT-doped WO_3 hydrogen sensors prepared by the E-beam method.

Acknowledgements

References

1. Korotcenkov, G.; Han, S.D.; Stetter, J.R. Review of electrochemical hydrogen sensors. *Chem. Rev.* **2009**, *109*, 1402-1433.
2. Moriarty, P.; Honnery, D. Hydrogen's role in an uncertain energy future. *Int. J. Hydrogen. Energ.* **2009**, *34*, 31-39.
3. Momirlan, M.; Veziroglu, T.N. The properties of hydrogen as fuel tomorrow in sustainable energy system for a cleaner planet. *Int. J. Hydrogen. Energ.* **2005**, *30*, 795-802.
4. Árnason, B.; Sigfússon, T.I. Iceland—A future hydrogen economy. *Int. J. Hydrogen. Energ.* **2000**, *25*, 389-394.
5. Carcassi, M.N.; Fineschi, F. Deflagrations of H_2-air and CH_4-air lean mixtures in a vented multi-compartment environment. *Energy* **2005**, *30*, 1439-1451.
6. Penza, M.; Tagliente, M.A.; Mirenghi, L.; Gerardi, C.; Martucci, C.; Cassano, G. Tungsten trioxide (WO_3) sputtered thin films for a NO_x gas sensor. *Sens. Actuat. B Chem.* **1998**, *50*, 9-18.
7. Wang, X.; Miura, N.; Yamazoe, N. Study of WO_3-based sensing materials for NH_3 and NO detection. *Sens. Actuat. B Chem.* **2000**, *66*, 74-76.
8. Kim, T.S.; Kim, T.B.; Yoo, K.S.; Sung, G.S.; Jung, H.J. Sensing characteristics of dc reactive sputtered WO_3 thin films as an NO_x gas sensor. *Sens. Actuat. B Chem.* **2000**, *62*, 102–108.

9. Sawicka, K.M.; Prasad, A.K.; Gouma, P.I. Metal oxide nanowires for use in chemical sensing applications. *Sens. Lett.* **2005**, *3*, 31-35.

10. Tao, W.H.; Tsai, C.H. H_2S sensing properties of noble metal doped WO_3 thin film sensor fabricated by micromachining. *Sens. Actuat. B Chem.* **2002**, *81*, 237-247.

11. Frühberger, B.; Grunze, M.; Dwyer, D.J. Surface chemistry of H_2S-sensitive tungsten oxide films. *Sens. Actuat. B Chem.* **1996**, *31*, 167-174.

12. Hoel, A.; Reyes, L.F.; Heszler, P.; Lantto, V.; Granqvist, C.G. Nanomaterials for environmental applications: Novel WO_3-based gas sensors made by advanced gas deposition. *Curr. Appl. Phys.* **2004**, *4*, 547-553.

13. Ionescu, R.; Hoel, A.; Granqvist, C.G.; Llobet, E.; Heszler, P. Low-level detection of ethanol and H_2S with temperature-modulated WO_3 nanoparticle gas sensors. *Sens. Actuat. B Chem.* **2005**, *104*, 132-139.

14. Li, X.; Zhang, G.; Cheng, F.; Guo, B.; Chen, J. Synthesis, characterization, and gas-sensor application of WO_3 nanocuboids. *J. Electrochem. Soc.* **2006**, *153*, 133-137.

15. Xu, Y.; Tang, Z.; Zhang, Z.; Ji, Y.; Zhou, Z. Large-scale hydrothermal synthesis of tungsten trioxide nanowires and their gas sensing properties. *Sens. Lett.* **2008**, *6*, 938-941.

16. Neri, G.; Micali, G.; Bonavita, A.; Ipsale, S.; Rizzo, G.; Niederberger, M.; Pinna, N. Tungsten oxide nanowires-based ammonia gas sensors. *Sens. Lett.* **2008**, *6*, 590-595.

17. Llobet, E.; Molas, G.; Molinàs, P.; Calderer, J.; Vilanova, X.; Brezmes, J.; Sueiras, J.E.; Correig, X. Fabrication of highly selective tungsten oxide ammonia sensors. *J. Electrochem. Soc.* **2000**, *147*, 776-779.

18. Balázsia, C.; Wang, L.; Zayim, E.O.; Szilágyid, I.M.; Sedlackováe, K.; Pfeifera, J.; Tótha, A.L.; Goumab, P.I. Nanosize hexagonal tungsten oxide for gas sensing applications. *J. Eur. Ceram. Soc.* **2008**, *28*, 913-917.

19. Wang, U.; Pfeifer, J.; Balazsi, C.; Gouma, P.I. Synthesis and sensing properties to NH_3 of hexagonal WO_3 metastable nanopowders. *Mater. Manuf. Process.* **2007**, *22*, 773–776.

20. Berger, O.; Hoffmann, T.; Fischer, W.J.; Melev, V. Tungsten-oxide thin films as novel materials with high sensitivity and selectivity to NO_2, O_3, and H_2S. Part II: Application as gas sensors. *J. Mater. Sci.: Mater. Electron.* **2004**, *15*, 483-493.

21. Aroutiounian, V. Metal oxide hydrogen, oxygen, and carbon monoxide sensors for hydrogen setups and cells. *Int. J. Hydrogen. Energ.* **2007**, *32*, 1145-1158.

22. Ahmad, A.; Walsh, J. Development of WO_3-based thick-film hydrogen sensors. *ECS Trans.* **2006**, *3*, 141-152.

23. Ippolito, S.J.; Kandasamy, S.; Kalantar-zadeh, K.; Wlodarski, W. Hydrogen sensing characteristics of WO_3 thin film conductometric sensors activated by Pt and Au catalysts. *Sens. Actuat. B Chem.* **2005**, *108*, 154-158.

24. Hsu, W.C.; Chan, C.C.; Peng, C.H.; Chang, C.C. Hydrogen sensing characteristics of an electrodeposited WO_3 thin film gasochromic sensor activated by Pt catalyst. *Thin Solid Films* **2007**, *516*, 407-411.

25. Fardindoost, S.; Iraji-zad, A.; Rahimi, F.; Ghasempour, R. Pd doped WO_3 films prepared by sol–gel process for hydrogen sensing. *Int. J. Hydrogen. Energ.* **2010**, *35*, 854-860.

26. Nakagawa, H.; Yamamoto, N.; Okazaki, S.; Chinzei T.; Asakura, S. A room-temperature operated hydrogen leak sensor. *Sens. Actuat. B Chem.* **2003**, *93*, 468-474.

27. Samarasekara, P. Hydrogen and methane gas sensors synthesis of multi-walled carbon nanotubes. *Chin. J. Phys.* **2009**, *47*, 361-369.

28. Zhu, L.; Xiu, Y.; Hess, D.W.; Wong, C.P. Aligned carbon nanotube stacks by water-assisted selective etching. *Nano Lett.* **2005**, *5*, 2641–2645.

29. Wongchoosuk, C.; Wisitsoraat, A.; Tuantranont, A.; Kerdcharoen T. Portable electronic nose based on carbon nanotube-SnO$_2$ gas sensors and its application for detection of methanol contamination in whiskeys. *Sens. Actuat. B Chem.* **2010**, *147*, 392–399.

30. Ansari, Z.A.; Ansari, S.G.; Ko, T.; Oh, J.H. Effect of MoO$_3$ doping and grain size on SnO$_2$-enhancement of sensitivity and selectivity for CO and H$_2$ gas sensing. *Sens. Actuat. B Chem.* **2002**, *87*, 105-114.

31. Lee, D.S.; Nam, K.H.; Lee, D.D. Effect of substrate on NO$_2$-sensing properties of WO$_3$ thin film gas sensors. *Thin Solid Films* **2000**, *375*, 142-146.

32. Hussain, O.M.; Swapnasmitha, A.S.; John, J.; Pinto, R. Structure and morphology of laser-ablated WO$_3$ thin films. *Appl. Phys. A: Mater. Sci. Process.* **2005**, *81*, 1291-1297.

33. Ashrit, P.V. Dry lithiation study of nanocrystalline, polycrystalline and amorphous tungsten trioxide thin-films. *Thin Solid Films* **2001**, *385*, 81-88.

34. Shinde, V.R.; Gujar, T.P.; Lokhande, C.D. LPG sensing properties of ZnO films prepared by spray pyrolysis method: Effect of molarity of precursor solution. *Sens. Actuat. B Chem.* **2007**, *120*, 551-559.

35. Zeng, Y.; Zhang, T.; Wang, L.; Kang, M.; Fan, H.; Wang, R.; He, Y. Enhanced toluene sensing characteristics of TiO$_2$-doped flowerlike ZnO nanostructures. *Sens. Actuat. B Chem.* **2009**, *140*, 73-78.

36. Sahay, P.P.; Nath, R.K. Al-doped zinc oxide thin films for liquid petroleum gas (LPG) sensors. *Sens. Actuat. B Chem.* **2008**, *133*, 222-227.

37. Liang, Y.X.; Chen, Y.J.; Wang, T.H. Low-resistance gas sensors fabricated from multiwalled carbon nanotubes coated with a thin tin oxide layer. *Appl. Phy. Lett.* **2004**, *85*, 666-668.

38. Bittencourt, C.; Felten, A.; Espinosa, E.H.; Ionescu, R.; Llobet, E.; Correig, X.; Pireaux, J.J. WO$_3$ films modified with functionalised multi-wall carbon nanotubes: Morphological, compositional and gas response studies. *Sens. Actuat. B Chem.* **2006**, *115*, 33-41.

39. Sakai, G.; Matsunaga, N.; Shimanoe, K.; Yamazoe, N. Theory of gas-diffusion controlled sensitivity for thin film semiconductor gas sensor. *Sens. Actuat. B Chem.* **2001**, *80*, 125-131.

40. Hieu, N.V.; Duc, N.A.P.; Trung, T.; Tuan, M.A.; Chien, N.D. Gas-sensing properties of tin oxide doped with metal oxides and carbon nanotubes: A competitive sensor for ethanol and liquid petroleum gas. *Sens. Actuat. B Chem.* **2010**, *144*, 450-456.

41. Wei, B.Y.; Hsu, M.C.; Su, P.G.; Lin, H.M.; Wu, R.J.; Lai, H.J. A novel SnO$_2$ gas sensor doped with carbon nanotubes operating at room temperature. *Sens. Actuat. B Chem.* **2004**, *101*, 81-89.

42. Cheong, H.W.; Lee, M.J. Sensing characteristics and surface reaction mechanism of alcohol sensors based on doped SnO$_2$. *J. Ceram. Process. Res.* **2006**, *7*, 183-191.

43. Lupan, O.; Ursaki, V.V.; Chai, G.; Chow, L.; Emelchenko, G.A.; Tiginyanu, I.M.; Gruzintsev, A.N.; Redkin, A.N. Selective hydrogen gas nanosensor using individual ZnO nanowire with fast response at room temperature. *Sens. Actuat. B Chem.* **2010**, *144*, 56-66.